Journal of Scientific Research
Banaras Hindu University, Varanasi

Vol. 56, 2012 : 197-216
ISSN : 0447-9483

HEAVY FLAVOR MEASUREMENT IN RELATIVISTIC HEAVY ION COLLISIONS

Sourav Tarafdar and Venktesh Singh
Department of Physics,
Banaras Hindu University, Varanasi 221 005, India

Abstract

In this paper a review of the measurement of heavy flavor to study the matter produced in High Energy Heavy Ion collision experiments has been given. We have also discussed the different results from few other experiments regarding the measurement of heavy flavor. More emphasis on PHENIX experiment has been given in this article.

1. Introduction

Since the discovery by Rutherford of nucleus, tremendous development has been made in order to understand the basic constituent of matter and the forces that bind them. Until 1960s, it was believed that basic constituent of nucleus was protons and neutrons. However Gell-Mann's theoretical proposal of quarks (having fractional charges of 2/3 and -1/3) being the constituent of protons made a huge revolution in High Energy Physics.

Several theories were proposed to understand the properties of these basic constituent of nature and the interaction between these quarks. The proposed theories made it possible to understand various combinations of quarks giving rise to large number of particles found in nature.

The first experiment in order to prove the existence of quarks inside the protons was Deep Inelastic Scattering (DIS) at SLAC in 1968. Due to Gell-Mann's theory being still under dispute at that time, the constituents found in DIS experiment were named partons. However later experiments in SLAC, Fermilab and elsewhere showed the partons having fractional charges of 2/3 and -1/3 and hence proving Gell-Mann's hypothesis to be correct.

The interaction between the quarks with each other happens by the exchange of another particle called gluon, which are neutral bosons. Both the quarks and gluons carry

charge termed as color charge analogous to electrical charge [1]. Unlike positive and negative charge in electrical case, the quarks (anti-quarks) and gluons carry color charges named red, blue and green. Quarks carry color, anti-quarks carry anti-color and gluons carry one color and one anti-color [2].

Now it is quite established that the basic constituent of nucleus is quarks bounded together by gluons however the complete understanding of the nature of force making the gluons to bind the quarks together has not yet been possible. In order to understand the nature of force making the gluons to bind quarks together, study of nucleon–nucleon collision is going on which is continuing to unfold this wonderful secret of nature.

One of the most interesting facts is that the interaction between quarks is completely opposite to the electromagnetic interaction. Unlike electromagnetic interaction the force of interaction between quarks decreases as they are brought close to each other, this phenomenon is called asymptotic freedom. Once they are brought sufficiently close to each other the quarks can unbound giving rise to the free quarks. This condition of free quarks can be achieved by bringing the quarks sufficiently close to each other which is possible if, either the temperature reaches of the order of the Sun's core temperature or the nuclear density becomes too high. No wonder why everything in nature is so stable.

It is believed that few microseconds (μs) after the Big Bang, the medium consisted of free quarks and gluons. This deconfined state of quarks and gluons is called Quark-Gluon Plasma (QGP). As mentioned earlier, this condition of free quark can be achieved only if we manage to bring quarks sufficiently close together. At energy density of $\varepsilon = 1$ GeV/fm^3 hadronic phase (confined quarks and gluons) undergoes phase transition and gives rise to QGP phase. Calculations based on lattice chromodynamics show us that this energy density can be achieved at a temperature of T = 170 MeV = 10^{12} K [3]. In laboratory, this condition can be achieved by head on smashing of heavy ions moving with the velocity of the order of light and this event is termed as relativistic heavy ion collisions.

There are many signals proposed by various models for detecting QGP. Some of the important signals are:

(i) Effect on nuclear stopping power due to creation of compressed hadronic matter. As the baryon rapidity distribution depends strongly on the baryon-baryon cross section [4], the change in nuclear stopping power due to compressed baryonic matter changes the shape of baryonic rapidity distribution.

(ii) Dilepton (lepton–anti-lepton pair) production makes it possible to understand the thermodynamic condition of the medium produced during heavy ion collisions. Interaction of quark and anti-quark inside QGP gives rise to virtual photon (γ^*) whichfurther decays into a lepton (l^-) and anti-lepton (l^+). Figure 1 shows the reaction $q + q \rightarrow l^+ + l^-$.

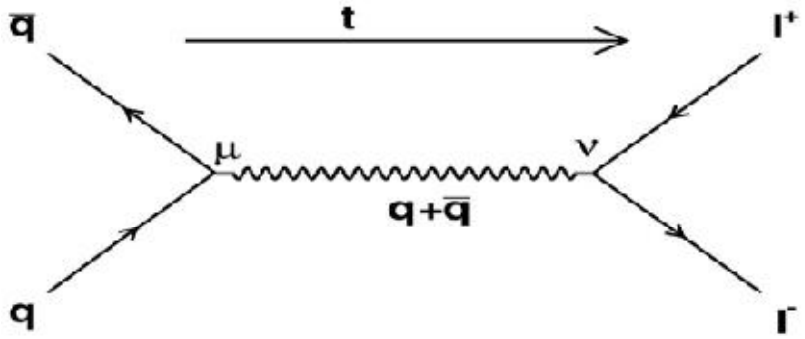

Fig. 1
Feynmann diagram for q + q → $l^+ + l^-$ reaction.
The vertices and the momentum of the lines are labeled.

The lepton and anti-lepton pair after their production passes through the collision region and as their mean free path is quite large they are not expected to undergo collisions after their production as well as their production rate and momentum distribution are dependent on the quarks and anti-quarks momentum distributions in the QGP which is governed by the thermodynamic condition of QGP [5 - 10]. Thus they carry the information of momentum distribution of quarks and antiquarks.

(iii) J/ψ suppression is caused by the Debye screening. This signature of QGP was proposed by Matsui and Satz [11]. Many theoretical [12-16] and experimental studies [17, 18] were performed on this phenomenon. Due to the presence of quarks, anti-quarks and gluons in QGP the color charge of quark is screened and this is termed as Debye screening. J/ψ being the bound state of c (charm) and anti-c, when present in the medium (produced during heavy ion collision) are found to be suppressed because of the weakened interaction between c and anti-c along with the vanishing of string tension between c and anti-c due to the deconfined quarks and gluons in QGP. However recent results on J/ψ measurement [18, 19] showed very different results than predicted by the models [20, 21] describing the Super Proton Synchrotron (SPS) data [17]. According to the models larger suppression of J/ψ at Relativistic Heavy Ion Collider (RHIC) compared to SPS and more suppression at mid rapidity than forward rapidity has been predicted. The J/ψ results at RHIC [18, 19] shows larger suppression at forward rapidity than at mid rapidity which cannot be explained by present models. The rapidity is a variable frequently used to describe the behavior of particles in inclusively measured reactions. It is defined by $y = ½ [\log \{(E + p_L) / (E - p_L)\}]$, which corresponds to $\tanh(y) = (p_L)/(E)$, where y is the rapidity, p_L is the longitudinal momentum along the direction of the incident particle, E is the energy, both defined for a given particle. Besides that

the spectral shape function of J/ψ calculated by using lattice QCD calculations has shown that J/ψ can survive above the critical temperature of the QGP phase transition [22, 23]. Thus currently J/ψ suppression study inrelativistic heavy ion collision is being used to study the property of QGP.

(iv) Photon production in QGP takes place due to the possible interaction amongst quark and anti-quark alongwith the production of gluon [24]. This process is called annihilation and can be represented by the equation $q + q \rightarrow \gamma + g$, where g is gluon. This process is represented in terms of Feynmann diagram by the top panel in Figure 2. Other than annihilation process a gluon interacting with a quark or anti-quark can also produce photon [24] which can be represented by the reactions $g + q \rightarrow \gamma + q$ and $g + q \rightarrow \gamma + q$ and the process is termed as the Compton scattering. Bottom panel of Figure 2 shows the Feynman diagram of the Compton scattering. Experimental studies [25, 26] were made by collider experiments on these photon productions in heavy ion collisions. The produced photon in the collision region interacts with the particles in that region via electromagnetic interaction, which being not so strong makes the mean free path of the photon large enough to avoid further interaction in the medium. Thus, the escaped photon from the collision region carries thermodynamical information about the medium produced in the collision region.

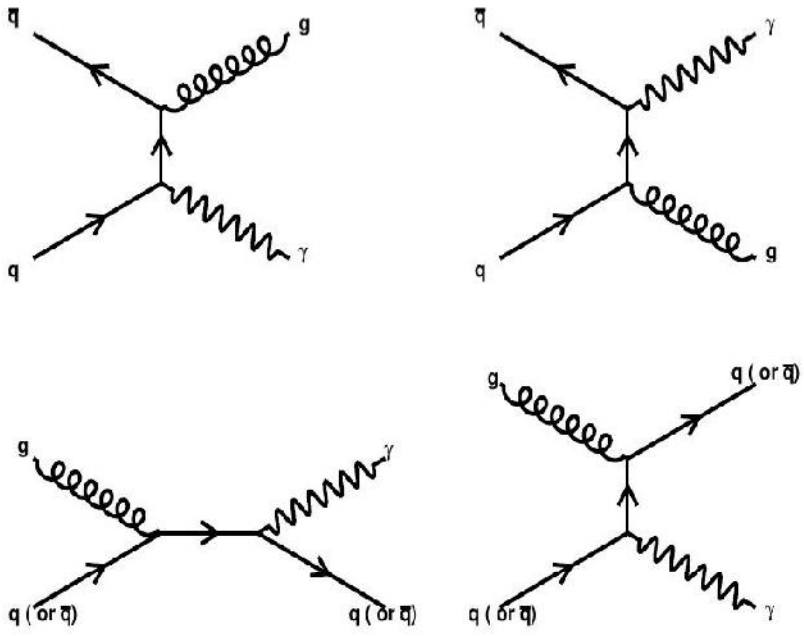

Fig. 2
Feynmann diagram for annihilation process (top panels) and for the Compton scattering (bottom panels).

(v) Strangeness production is a signature and a diagnostic tool of QGP formation and properties. Unlike up and down quarks, from which everyday matter is made, strange quarks are formed in pair production processes in collisions between constituents of the plasma. The dominant mechanism of production involves gluons only present when matter has changed into the QGP phase. When QGP disassembles into hadrons in a breakup process, the high availability of strange anti-quarks helps to produce antimatter containing multiple strange quarks, which is otherwise rarely made. Similar considerations are at present made for the heavier charm quark flavor which is made earlier on at the beginning of the collision process in first interactions and is only abundant in the high-energy environments. We can not assume that under all conditions the yield of strange quarks is in thermal equilibrium. Therefore, strangeness enhancement is expected to take place in case of existence of QGP [27-33]. In QGP, collisions amongst the constituents of the medium can produce strange quarks and antiquarks. Interaction amongst light quarks and anti-quarks can produce strange quarks and anti-quarks as shown in Figure 3. Other than this, collisions amongst the gluons in the medium can also produce strange quarks and anti-quarks. Schwinger factor [34, 35] describes the charm production rate under the non existence of chemical equilibrium. The mass dependence of this factor (Aexp[−k mq], where, A and k being constants and mq being quark mass) shows that heavy quarks (like strange quarks) are suppressed due to the absence of chemical equilibrium. However during QGP phase when chemical equilibrium is achieved there is enhancement in the production of strange quarks.

Thus, considering the above mentioned signatures of QGP the important probes for determining them are photons, dileptons and leptons. The leptons from heavy flavor decays as described earlier is an important tool for understanding the nature of medium produced during the heavy ion collisions.

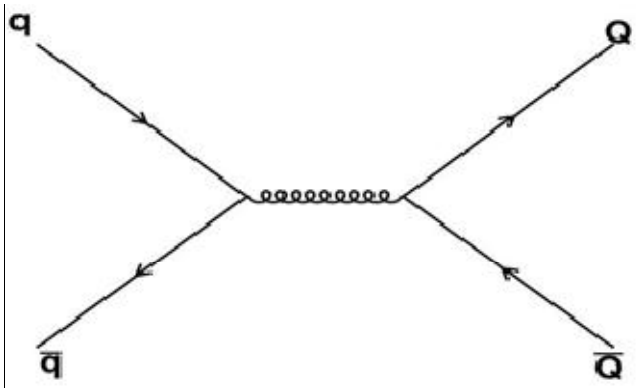

Fig. 3
Feynmann diagram for strangeness production. q and q are the light quarks and anti-quarks whereas the Q and Q are the heavy quarks and anti-quarks like strange quarks and anti-quarks.

2. Experimental Scenario

The Relativistic Heavy Ion Collider (RHIC) at Brookhaven National Laboratory (BNL) is dedicated to study the nuclear matter under extreme condition and to explore the phase diagram of strongly interacting matter for new state of matter. This research presents themeasurement of single electron from heavy flavor decay from d + Au collisions at √SNN = 200 GeV collected during the 2008 RHIC run with PHENIX (Pioneering High Energy Nuclear Interaction Experiment) detector and calculates the nuclear modification factor for d + Au collisions.

RHIC is capable of colliding nuclei from p + p to Au + Au across a wide range of collision energies from center of mass energy per nucleon – nucleon collision of $\sqrt{S_{NN}}$ = 22 GeV to $\sqrt{S_{NN}}$= 200 GeV for Au + Au. For p + p the collision energy is capable of going up to $\sqrt{S_{NN}}$ = 500 GeV.

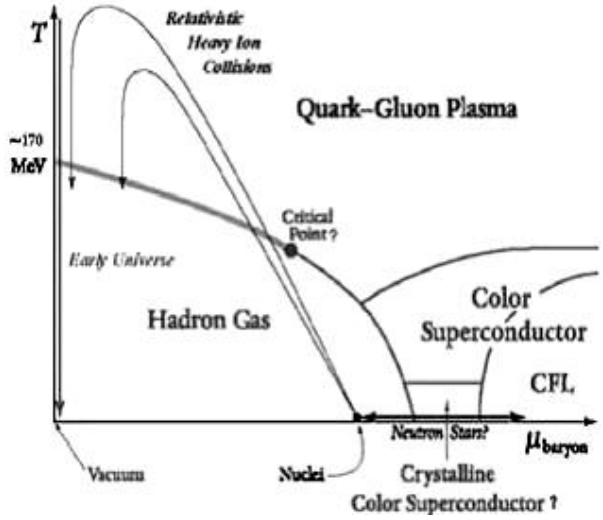

Fig. 4
Conjectured QCD phase diagram.

Figure 4 shows the conjectured phase diagram [36, 37] of QCD matter as a function of temperature (T) and baryon chemical potential (μ_{baryon}). In the bottom left-hand corner of the phase diagram both T and μ_{baryon} are small and the quarks and anti-quarks combine with each other giving rise to hadrons. We may call this region as hadronic phase. According to Lattice QCD calculation at about T = 175 MeV [38, 39] there may occur phase transition where quarks may be found in deconfined state giving rise to the medium called QGP. The exact location of the critical point and the exact order of phase transition are not yet fixed but from the experimental data [40] it is confirmed that RHIC has the ability to explore the region where the quarks and gluons are being found in

thedeconfined state. According to the theoretical calculations the required energy density for a QCD phase transition is of the order of 1 GeV /fm^3 [41]. The RHIC collisions produce energy densities of the order of 5 GeV /fm^3 [40] showing RHIC has the ability to explore the new state of matter.

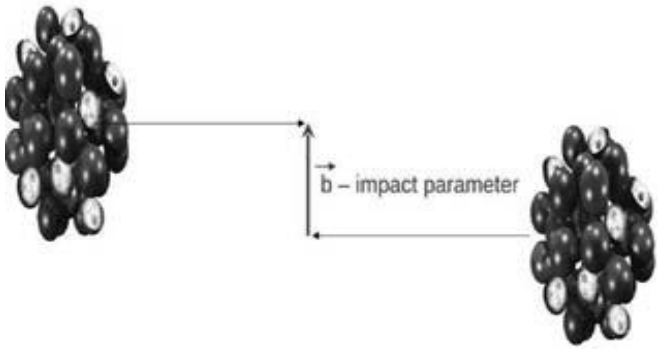

Fig. 5
Schematic diagram of the impact parameter (b). Ions from both sides are moving towards each other at relativistic velocity.

Heavy ion collisions are being described by parameter called impact parameter (b) shown in Figure 5. Impact parameter can be defined as the distance between the center of two nuclei colliding with each other and it basically gives us the information of overlap region of the colliding nuclei. Collisions with smallest b are referred as the most central collisions whereas the ones with large b are termed as peripheral collisions.

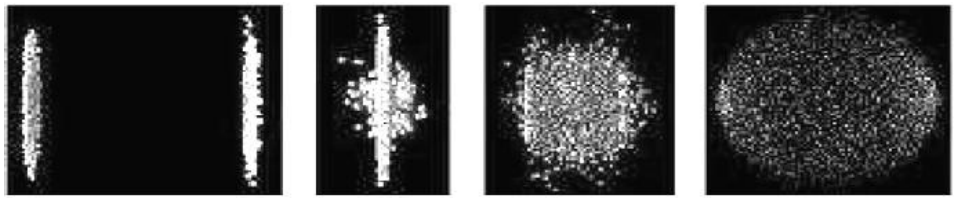

Fig. 6
Schematic steps of heavy-ion collision from left (initial) to right (final).

Two ions traveling towards each other with the velocity of the order of the velocity of light seems to be contracted because of Lorentz contraction. The two ions during collision smash into one another and then pass through each other. Intense high temperature is produced making the quarks and gluons to unbind for a brief period of time. Just after collision the area cools off causing the quarks to recombine and form several particles detection of which gives us the glimpse of the properties of the matter produced during the, collision process. Successive steps of the above mentioned process is shown in Figure 6.

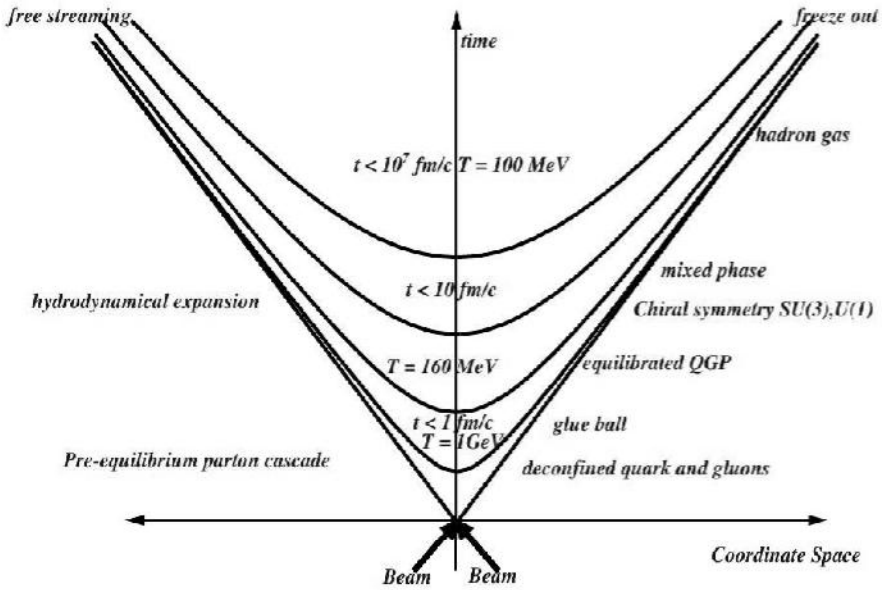

Fig. 7
Schematic diagram of space – time evolution in nucleus – nucleus collision where QGP is expected to form.

Figure 7 shows the schematic of the heavy ion collision where QGP is expected to form. As shown in the figure after the initial collision of heavy ions, parton production is expected within a time of 1 fm/c. The system begins to expand and cool down because of the pressure making the local density go below the threshold for phase transition and according to QCD the partons become confined within hadrons. Figure 7 is the schematic space-time diagram of the nucleus–nucleus collision. It shows the time scale of the various stages of medium produced after the collision takes place. Freeze out in the Figure 7 is referred as the incidence when the interaction between the hadrons stops. The hadron–gas produced after collision continues to expand and interact until chemical freeze-out where the hadrons stops interacting inelastically. After further expansion and cooling, the last elastic interaction happens and thermal freeze-out occurs. The hadrons then undergo decaying mechanism following their known modes of decay which can be detected experimentally.

3. Heavy Quark production and its role as a probe for matter produced at RHIC

Heavy quarks are one of the most valuable probes for the matter produced at RHIC collisions mainly because of their masses (mc ≈ 1.3 GeV, mb ≈ 4.2 GeV) being quite large than the typically attained ambient temperatures or other non-perturbative scales, $m_Q >> T_C$, Λ_{QCD} = 0.2 GeV^3 [42]. The mass scale of heavy quarks causes: (i) the

production of heavy quarks constrained to the early, primordial stages of heavy ion collision and (ii) delay in thermalization of heavy quarks relative to light quarks. It is expected that the heavy quarks full thermalization time scale is longer than the life time of QGP resulting in retaining the information of the interaction history.

Table 1

Experimental and theoretical estimates of Heavy quark cross-sections are tabulated. The PHENIX data and theoretical values are for $\sqrt{S_{NN}}$ = 200 GeV in p + p collisions. The STAR data is for d + Au measurement.

Quarks	σ_{total} (mb)	Uncertainty on σ	Sources
charm	0.244	+0.381 / -0.134	NLO [43]
charm	1.3	±0.2stat ± 0.4sys	STAR [44]
charm	0.256	+0.400 / -0.146	FONLL [45]
charm	0.567	±0.057stat ± 0.224sys	PHENIX [46]
bottom	0.00187	+0.00099 / -0.00067	FONLL [45]
bottom	0.0046	±0.0013stat + 0.0026/ −0.0022sys	PHENIX [47]
bottom	0.0039	±0.0025stat + 0.003/ − 0.002sys	PHENIX [48]

RHIC energy is sufficient to produce heavy quarks, primarily for charm production.Bottom is also produced; however, the total production of bottom is significantly lower than that of charm production. It has been estimated that the total bottom cross-section is about 1-2% of the total charm cross-section. The specific values are tabulated in Table 1. PHENIX measurement shows that for $\sqrt{S_{NN}}$ = 200 GeV p + p collisions, the charm crosssection exceeds the bottom cross-section until $p_T \sim 4.0$ GeV/c, above which bottom dominates [49].

Different decay channels are used for detecting the heavy flavor hadrons. In the presentwork the measurement of the spectra of heavy flavors is based on the measurement of the spectra of heavy flavor electrons and positrons $[(e^+ + e^-)/2]$ from the semi-leptonic decays like $D^0 \rightarrow K^- + e^+ + \nu_e$, $D^+ \rightarrow K^0 + e^+ + \nu_e$ etc. Figure 8 shows the two decay channels of experimental interest in PHENIX. The center of the figure shows the charm (c) / anticharm (anti-c) quark pair produced in an initial inelastic hard collision. The right hand D^0 decay channel shows the hadronic decay to $K + \pi^-$. This hadronic decay mode is used for the study of charm production which is not the focus of this article. The left hand D^0 decay mode shows the semi-leptonic decay of D^0 to a lepton, the lepton's anti-neutrino and a K^-.

The quantity nuclear modification factor, in heavy ion collisions provides us the information regarding the effects of medium on the particle yield. The nuclear

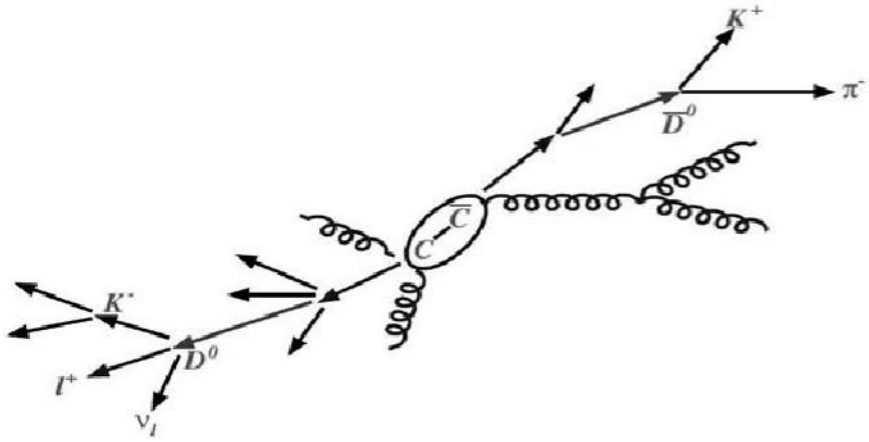

Fig. 8
Fragmentation of charm quark and semi-leptonic decay of charm meson.

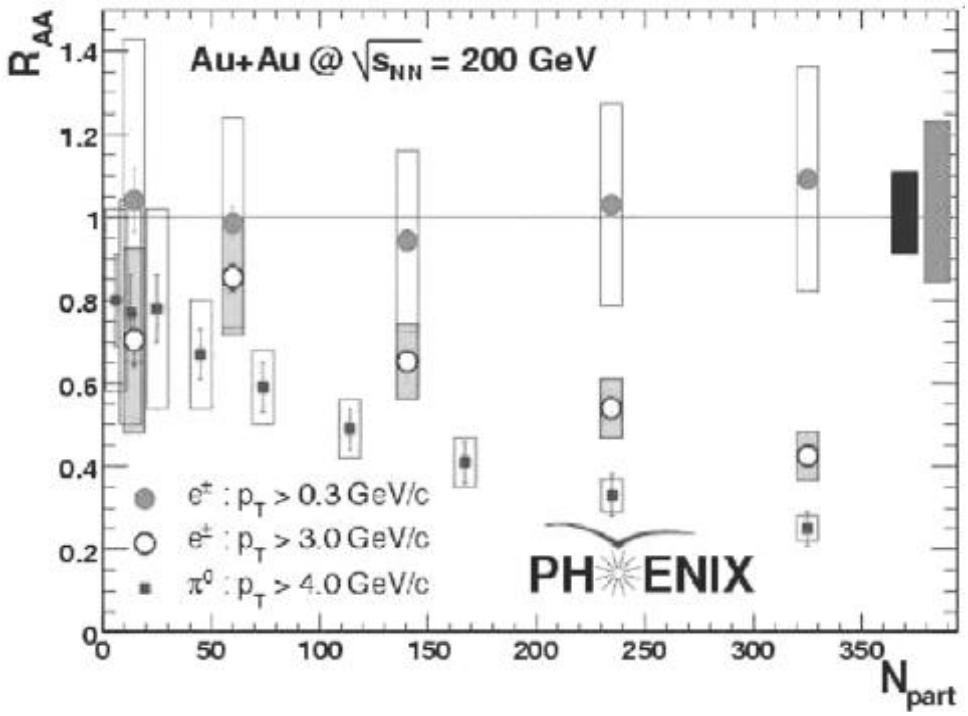

Fig. 9
Nuclear modification factor of light and heavy quarks as a function of number of participants N_{part} [50].

ABBYY PDF Transformer 2.0 Click here to buy www.ABBYY.com

modification factor is defined as the ratio between the particle yield in particular heavy ion collisions (dN_{A+B}) to the particle yields in binary nucleon–nucleon collisions (dN_{p+p}) scaled by the expected number of point-like binary nucleon–nucleon collisions $<N_{coll}>$, for the centrality class considered. Thus nuclear modification factor, R_{AB} is

$$R_{AB} = \frac{dN_{A+B}}{<N_{coll}>dN_{p+p}} \quad (1)$$

The measurement of invariant differential yield / cross-section for p + p provides the baseline for the physics conclusion from the measurement of R_{AB} for other heavy-ions collision species. One of the most interesting experimental results at RHIC is that of the significant energy loss of light quarks observed in the QGP like medium. The light quarks are being observed through light mesons measurement like π0 while the heavy quarks are observed by single leptons.

Figure 9 shows the nuclear modification factor, R_{AA}, in Au + Au for both light meson (π^0) and heavy quarks (single electrons from decay channel of D's) for selected p_T bins as a function of N_{part}. N_{part} is the number of participants in heavy-ion collisions and gives us the idea of collision centrality. The filled rectangle points in the Figure 9 shows that R_{AA} is decreasing with increasing N_{part} (moving towards more central collision) for light mesons showing significant energy loss of the light quarks in the medium produced due to Au + Au collision.

Gluon radiation (emission of gluons due to acceleration of quarks) and elastic – inelastic scattering of quarks in the medium can explain the quark energy loss within the medium. The filled circle points in Figure 9 shows the R_{AA} for heavy flavor single electron with $p_T > 0.3$ GeV/c. For $p_T > 0.3$ GeV/c, there contains more than half of the heavy flavor decay electrons and the $R_{AA} = 1.0$ is consistent with the binary scaling of total heavy-flavor yield.

The open circle points in above Figure shows the R_{AA} for heavy flavor single electron with $p_T > 3.0$ GeV/c and one can see the suppression in R_{AA} with the increase in N_{part}. Comparing this with the R_{AA} for π^0 (filled rectangular points) it can be seen that the heavy quarks looses less energy than the light quarks but still it is greater than originally expected when taking into account dead cone effect [51]. The observed energy loss is yet to be understood fully. However the clear suppression of R_{AA} for Au + Au collision clearly shows medium is produced which is absent in p + p collision.

4. Measurement of Heavy Flavor cross-sections using FONLL

FONLL [45] which stands for Fixed-Order plus Next-to-Leading-Log, provides the means to calculate the heavy flavor single lepton p_T spectrum, $Ed\sigma_l$ and also the total

production cross-section σ_{hv}. The heavy flavor single lepton p_T spectrum determined from FONLL can be directly compared with the measurement.

$$E\frac{d^3\sigma_1}{dp^3} = \frac{E_Q d^3\sigma_Q}{dp_Q^3} \otimes D\left(Q \to H_Q\right) \otimes f\left(H_Q \to \ell\right) \quad (2)$$

The factorized lepton production cross-section can be given schematically in equation (2) where, $\otimes$ in the above expression denotes a generic convolution. It is to be noted that the above schematic expression of lepton spectrum consists of three main components. These are (i) $E_Q d^3\sigma_Q / dp^3_Q$; heavy quark (Q), p_T and rapidity distri-butions at $\sqrt{S_{NN}}$ = 200 GeV which is calculated in perturbative QCD, (ii) (Q → HQ); heavy quarks fragmentation into heavy hadrons (H_Q) which is described by the phenomenological input extracted from $e^+ e^-$ data and (iii) f (HQ → l); the electron decay spectrum term where the heavy hadrons (HQ) decays into electrons. The spectrum for this case is available from other measurements.

The FONLL calculation apart from including the full fixed-order NLO result [52–55], also resumes [56] the large perturbative terms proportional to $\alpha^n_S \log^k (p_T / m)$. The resummation is done to all orders with next-to-leading logarithmic (NLO) accuracy (i.e., k = n, n − 1) where the heavy quark mass is denoted by m here. The heavy quark by FONLL is being treated as an active light flavor for $p_T >> m$. Thus, the number of light flavors for calculation of α_s in FONLL is 4 for charm and 5 for bottom while in NLO calculation the produced heavy quark is not active flavor, so the α_s is calculated with n_{1f} = 3, 4 for charm and bottom respectively.

The parameters for FONLL calculation includes the heavy quark mass and the value of strong coupling, α_s. These two terms are the perturbative parameters. Apart from these perturbative parameters the FONLL calculation depends on unphysical factorization (μ_F) and renormalization (μ_R) scales. The central values of these scales is given by $\mu_F = \mu_R = \mu_o = \sqrt{(p_T^2 + m^2)}$. In order to get the uncertainty the two scales (μ_R and μ_F) are varied independently within fiducial region as described in [45].

5. Methodology of Heavy Flavor Measurements in PHENIX

Charm quarks produced in the initial hard scattering processes between partons will hadronize into the family of open charm D mesons, which are combinations of rare c or anti-c quarks with other light mesons. The fragmentation function describes the energy distribution of the final state D meson which is the fraction of energy inherited from the original c-quark. Both hadronization and fragmentation can only be measured experimentally.

The non-conservation of the charm quantum number in weak interaction causes the single charm quark, D's decay weakly with the lifetime of $\tau \approx 10^{-15}$ seconds. Figure 8 is an example of the weak, semi-leptonic decay of a D meson where the resulting single

lepton is either an electron or muon. The semi-leptonic decay of D mesons has been widely discussed in literature [57–67].

According to the weak interaction theory, certain decay modes of D mesons are highly favored than others. Other than the single lepton semi-leptonic decay mentioned earlier, other prominent decay modes like $D^0 \rightarrow K^- + \pi^+$ [68] and $D^+ \rightarrow K^- + \pi^+ + \pi^-$ [69] result in light hadron daughters. Both semi-leptonic decay channels and light hadron decay channels are the convenient methods for measuring heavy quark production from heavy flavor mesons. Measurement using light hadron decay channels corresponds to the direct measurement as one can observe the D's as a peak from the invariant mass spectrum of the hadron daughters produced from the decay of D mesons. The semi-leptonic decay mode corresponds to indirect measurement as leptons are measured and it is used to infer the D meson and by extension the charm quark. The indirect method of heavy flavor measurement is the procedure employed in this research work. Here the observable is single electrons from the semi-leptonic decay of D mesons. The analysis procedure employed here to measure the single electrons is well established method [70]. The indirect method involves the measurement which is statistical in the sense it involves estimation of all backgrounds and then they got subtracted from all single lepton candidate tracks detected by the detector. Only after understanding the primary sources of backgrounds properly they are subtracted and the leftover particle tracks are attributed to the heavy flavor signal. In this method one cannot identify a particular track as a background or a heavy flavor signal. It's only through the statistical estimation and subtraction of quantities that one can obtain any relevant physical quantity.

6. Overview of Heavy Flavor measurement by PHENIX

The PHENIX detector, instead of having full 4π coverage is designed to make measurements in two major kinematics regions. The two regions, according to the convention of measuring the angles relative to the beam axis, are: a) mid-rapidity, with $\pi/2$ acceptance centered at 90° polar angle in the central arm and b) forward rapidity from about 10° to 30° polar angle in both forward and backward directions with full azimuthal coverage. Figure 10 shows the schematic layout of PHENIX detector.

The PHENIX detector weighs 4,000 tons and is a collection of several small and large sized detectors, each performing a specific role during collection of data from RHIC collision. Figure 10 shows the layout of the PHENIX detector. The detectors are grouped into two central arms, two muon arms and event characterization detectors. Central arms have detectors meant for measuring particles like pions, protons, Kaons, deuterons, photons and electrons. Muon arms are dedicated for measuring muon particles and the event characterization detectors provide information about collision centrality and event vertex. Other than these a set of three huge magnets are used for bending the trajectories of the charged particles.

The central arm has particle identification detectors and has very low material within their acceptance making them to focus on the measurement of electrons. The particle

identification detectors enable PHENIX to collect clean sample of electrons. However other than electrons from heavy flavor decay, several other sources also contributes to the electrons being detected by PHENIX detector. The $\pi^0 \rightarrow \gamma + \gamma$ decay and the subsequent photon decay have the maximum contribution towards the electron background. Dalitz decay also has significant contribution towards the electron.

Direct photons, weak kaon decay and vector meson decay are the other less important sources of background electrons. Most of these background sources mainly π^0 and η, have been independently measured by PHENIX detector providing an excellent input to the Monte Carlo detector simulation for the determination of background contribution [71]. These contributions are well understood electromagnetic processes. The photon conversion contribution background is measured by adding extra conversion material in PHENIX detector acceptance and increment in the conversion takes place by a well determined factor. All these details when combined together give precise information of the background in heavy flavor measurement.

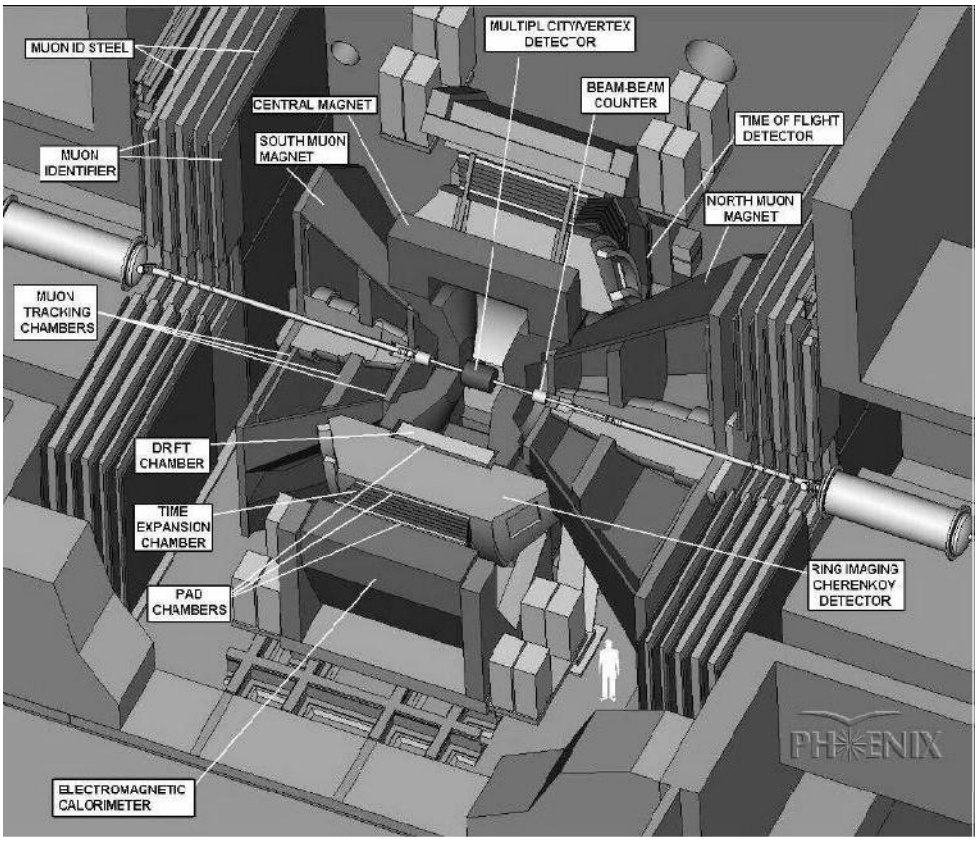

Fig. 10
Layout of PHENIX detector.

Until 2010 PHENIX detector is unable to separate the charm and bottom decays. The installation of Silicon Vertex Trackers (VTX) [72] provides the accurate measurement of the collision vertex as well as secondary vertex decay. The installation of VTX has been done during 2011. The installation of VTX will help to clearly distinguish the decays from charm and bottom in central arm of PHENIX. Thus the future measurement of heavy flavor will be of greatly improved quality as it will be possible to clearly distinguish between prompt decays and off-vertex decays of charmed and bottom meson.

7. Overview of Heavy Flavor Measurement in Large Hadron Collider (LHC)

Four important experiments are operational at LHC. These are ATLAS, ALICE, CMS and LHCb. All these four experiments are capable of studying heavy flavor production at LHC. The four experiments are designed to work in different luminosity conditions.

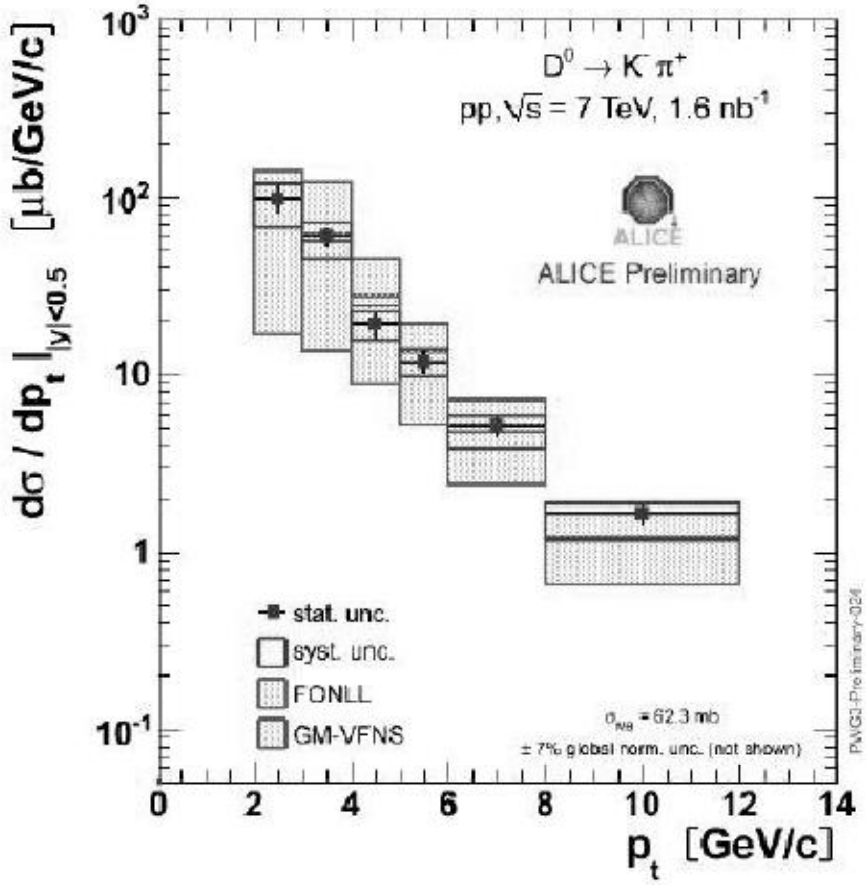

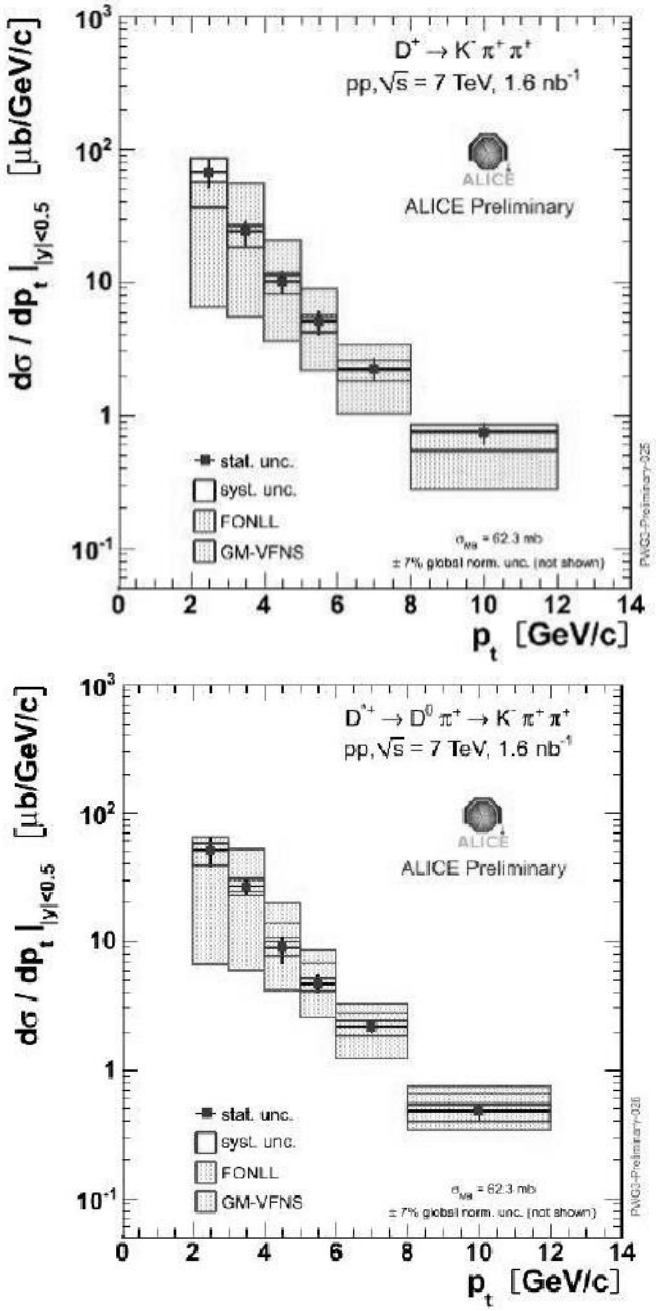

Fig. 11
D meson cross-section measured by Alice for D^o, D^+ and D^- [73].

Figure 11 shows the cross-section measured by Alice for D mesons (D^0, D^+, D^-).

ATLAS and CMS has the capability to work in wide luminosity range upto $10^{34}cm^{-2}s^{-1}$ while ALICE has the design to work at 3×1030 $cm^{-2}s^{-1}$. LHCb has optimal luminosity range $(2\text{-}5)\times10^{32}$ $cm^{-2}s^{-1}$. As ALICE has acceptance down to very low p_T so it is expected to play very important role. All the four experiments are using the direct detection strategy which involves identification of single tracks or vertices displaced from the interaction vertex and are based on the life time order (~ ps) for D mesons and B mesons. Importance to the identification of both lepton and hadron has been given for heavy flavor detection in all the four experiments in LHC. Both D and B mesons has relatively large branching ratios in the semi-leptonic channels. High p_T leptons are being used as trigger level tags to select $B \rightarrow J/\psi + X$ candidate events which provide more accurate cross-section measurements.

ALICE can identify electrons with $p_T > 1$ GeV and $|\eta| < 0.9$, via transition radiation and dE/dx measurements, and muons in the forward region, $2.5 < \eta < 4$, which allows a very low p_T cutoff of 1 GeV. CMS and ATLAS have broad pseudorapidity coverage for muons, $|\eta| < 2.4$ and $|\eta| < 2.7$, respectively, but they have a higher p_T cutoff varying between 4 and 6 GeV, depending on η. Both CMS and ATLAS have high-resolution electro-magnetic calorimeters that are being used to identify electrons. Semi-leptonic inclusive measurements do not provide direct information on the D (B)-meson p_T distribution, especially at low p_T, because of the weak correlation between the lepton and the meson momenta. Thus, particularly for charm, the reconstruction of hadronic decays is preferred. At low p_T, hadron identification allows more effective mean to reject combinatorial background.

8. Conclusion

Thus, taking a look into the current experimental status of different experiments at RHIC (PHENIX and STAR) and LHC (ATLAS, ALICE, CMS, LHCb) the heavy flavormeasurement and study is an interesting aspect in order to understand the quark gluon plasma. With the continuous up gradation of different detectors in the different experiments, the future of heavy flavor measurement is very bright and it is expected to shed more light on the hot and dense matter produced in heavy ion collisions.

Acknowledgment

Author Mr. S. Tarafdar is thankful to the University Grant Commission (UGC), New Delhi for providing financial support through out the period of his research.

REFERENCES

1. Donald, H. Perkins: Introduction to High Energy Physics (Addison-Wesley), chap. History and Basic concepts, pp. 26-29.

2. R. Nave: The Color Force, Hyper Physics. Georgia Sate University, Department of Physics and Astronomy, retrieved 26-4-2009.

3. F. Karsh: Lectures on Quark Matter (Pringer, Berlin, Germany, 2002), vol. 583 of Lecture Notes in Physics, chap. Lattice QCD at high temperature and density, pp. 209-249, ISBN 978-3-540-43234-0.

4. M. Berenguer *et al*., (1992): *J. Phys*., G, 18, p. 655.

5. E. V. Shuryak, (1978): *Phys. Lett*., B, 78, 150.

6. K. Kajantie and H. I. Miettinen, Z. (1981): *Phys*., C, 9, p. 341.

7. K. Geiger and J. I. Kapusta, (1993): *Phys. Rev. Lett*., 70, p. 1920.

8. E. Shuryak and L. Xiong, (1993): *Phys. Rev. Lett*., 70, p. 2241.

9. B. Kampfer and O. P. Pavlenko, (1992): *Phys. Lett*., B, 289, p.127.

10. J. I. Kapusta, L. MacLerran, D. K. Srivastava, (1992): *Phys. Lett*., B, 283, p. 145.

11. T. Matsui and H. Satz, (1999): *Phys. Rep*., 310, p. 197.

12. R. Voigt, Phys. (1999): *Rep*., 310, p. 197.

13. B. Zhang, C. M. Ko, B. A. Li, Z. W. Lin and B. H. Sa, (2000): *Phys. Rev*., C, 62, 054905.

14. B. Zhang, C. M. Ko, B. A. Li, Z. W. Lin and S. Pal, (2002): *Phys. Rev*. C, 65, 054909.

15. X. Zhao and R. Rapp, (2008): *Phys. Lett*., B 664, 253.

16. L. Yan, P. Zhuang, and N. Xu, (2006): *Phys. Rev. Lett*., 97, 232301.

17. B. Alessandro *et al*. (2005): (NA50 Collaboration), *Eur. Phys. J*., C, 39, 335.

18. A. Adere *et al*. (2007): (PHENIX Collaboration), *Phys. Rev*. Lett., 98, 232301.

19. A. Adere *et al*. (2011): (PHENIX Collaboration), *Phys. Rev*., C, 84, 054912.

20. L. Grandchamp *et al*., (2004): *Phys. Rev. Lett*., 92, 212301.

21. A. Capella and E.G. Ferreiro, (2005): *Eur. Phys. J*. C, 42, p. 419.

22. M. Asakawa and T. Hatudsa, (2004): *Phys. Rev. Lett*., 92, 012001.

23. S. Datta, F. Karsch, P. Petreczky and I. Wetzorke, (2004): *Phys. Rev.*, D 69, 094507.

24. S. Y. Wang, D. Bayanovsky and K. W. Ng, (2001): arXiv:hep-ph/0101251v2.

25. S. S. Adler *et al*. (PHENIX Collaboration), (2007). *Phys. Rev. Lett*., 98, 012002

26. S. Abachi *et al*. (D0 Collaboration), (1996): *Phys. Rev. Lett*., 77, p. 5011.

27. P. Koch, B. Muller and J. Rafelski, (1986): *Phys. Rep.*, 142, p. 167.

28. J. Letessier, A. Tounsi, U. Heinz, J. Sollfrank and J. Rafelski, (1995): *Phys. Rev*., D 51, p. 3408.

29. M. N. Asprouli, A. D. Panagiotou, (1995): *Phys. Rev*., C, 51, p. 1444.

30. C. P. Singh, (1987): *Phys. Lett*., B, 188, p. 369.

31. C. P. Singh and S. Uddin, (1990): *Phys. Rev*., D 41, p. 870.

32. T. S. Biro, J. Zimanyi, (1983): *Nucl. Phys*., A, 395, p. 525.

33. P. Koch, (1991): *Prog. Nucl. Part. Phys*., 26, p. 253.

34. C. Y. Wong, (1994): Introduction to High Energy Heavy-Ion collisions, World Scientific.

35. C. Y. Wong, (1994): Introduction to High Energy Heavy-Ion collisions, World Scientific, Chapter 2, pp.19.

36. K. Rajagopal, (1999): *Nucl. Phys*., A, 661, p. 150.

37. J. Peter *et al*., (2007): arXIV:0705, p. 1930.

38. F. Karsch, (2004): *Prog. Theor. Phys. Suppl*., 153, p. 106.

39. F. Karsch, E. Laermann, and A. Peikert, (2001): *Nuclear Physics*, B 605, p. 579.

40. K. Adcox *et al*., (2005): *Nuclear Physics*, A, 757, p. 184.

41. F. Karsch, (2002): *Nucl. Phys*., A, 698, p. 199.

42. W. K. Tung, (2001): Perturbative qcd and the parton structure of the nucleon, (www.physics.smu.edu/~olness/cteqpp/tung2003/IntroPqcd.pdf).

43. R. Vogt, (2003): *Int. J. Mod. Phys*., E 12, p. 211.

44. J. Adams *et al*. (2005): (STAR Collaboration), *Phys. Rev. Lett*., 94, 062301

45. Matteo Cacciari, Paolo Nason and Ramona Vogt, (2005): *Phys. Rev. Lett*., 95, 122001.

46. A. Adare *et al*. (2006): (PHENIX Collaboration), *Phys. Rev. Lett.*, 97, 252002.

47. Y. Morino (2008): (PHENIX Collaboration), arXiv:0805, p. 3871.

48. A. Adare *et al*. (2008): (PHENIX Collaboration), arXiv:0802.0050.

49. A. Adare *et al*. (2009): (PHENIX Collaboration), *Phys. Rev. Lett.*, 103, 082002.

50. A. Adere *et al*. (2007): (PHENIX Collaboration), *Phys. Rev. Lett*. 98, 172301.

51. Yu. L. Dokshitzer and D. Kharzeev, (2001): *Phys. Lett*., B 519, p. 199.

52. P. Nason, S. Dawson, and R. K. Ellis, (1988): *Nucl. Phys*., B 303, p. 607.

53. P. Nason, S. Dawson, and R. K. Ellis, (1989): *Nucl. Phys*., B 327, p. 49.

54. P. Nason, S. Dawson, and R. K. Ellis, (1990): *Nucl. Phys*., B, 335, 260 (E).

55. W. Beenakker *et al*., (1991): *Nucl. Phys*. B, 351, p. 507.

56. M. Cacciari and M. Greco, (1994): *L. Nucl. Phys*. B, 421, p. 530.

57. A. Ali and T. C. Yang, (1976): *Phys. Lett*. B, 65, p. 275.

58. I. Hinchliffe and C. H. Llewellyn Smith, (1976): *Nucl. Phys*., B, 114, p. 45.

59. F. Bletzacker, H. T. Nieh and A. Soni, (1977): *Phys. Rev*., D, 16, p. 732.

60. W. J. Wilson, (1977): *Phys. Rev*. D, 16, p. 742.

61. V. Barger, T. Gottschalk and R. J. N. Phillips, (1977): *Phys. Rev.* D 16, p. 746.

62. D. Fakirov and B. Stech, (1978): *Nucl. Phys*., B, 133, p. 315.

63. X. Y. Pham and J. M. Richard, (1978): *Nucl. Phys*., B, 138, p. 453.

64. K. Kudoh, (1978): *Prog. Theor. Phys*., 60, p. 1834.

65. M. Suzuki, (1978): *Nucl. Phys*. B, 145, p. 420.

66. N. Cabibo, G. Corbo and L. Maiani, (1979): *Nucl. Phys.*, B, 155, p. 93.

67. M. Gluck, (1979): *Phys. Lett*., B, 84, p. 459.

68. C. Amsler *et al*. (2008): (Particle Data Group), *Phys. Lett*., B, 667, p. 1.

69. D. Drijard *et al*., (1979): *Phys Lett*., B, 81, p. 250.

70. J. A. Appel *et al*., (1974): *Phys. Rev. Lett*., 33, p. 722.

71. S. Tarafdar, P. K. Khandai and V. Singh, *Nucl. Phys*., A 862, 304 (2011); P. K. Khandai, P. Shukla and V. Singh, (2011): *Phys. Rev*., C, 84, 054904.

72. Y. L. Dokshitzer and D. E. Kharzeev, (2001): *Phys. Lett*., B, 519, p. 199.

73. A. Gelli (2011): (Alice Collaboration), *Journal of Physics*: Conference Series 316, 012025.